JOURNAL OF SOLID STATE CHEMISTRY 96, 344–359 (1992)

Structural and Electrical Studies of Mixed Copper/Ruthenium Oxides and Related Compounds of Zinc and Antimony

M. P. ATTFIELD, P. D. BATTLE,* S. K. BOLLEN, S. H. KIM, A. V. POWELL, AND M. WORKMAN

Inorganic Chemistry Laboratory, South Parks Road, Oxford, OX1 3QR, England

Received May 30, 1991; in revised form July 29, 1991

The preparation and characterization of a number of mixed metal oxides of ruthenium and copper are described, the compounds being chosen to demonstrate the changes that occur on moving from the 3-D perovskite structure to the 2-D K_2NiF_4 structure via the intermediate Ruddlesden–Popper structure. Full structure refinements by neutron powder diffraction are reported for $SrLaCuRuO_6$, $SrLaCuSbO_6$, $Sr_3NdCuRuO_8$, $Sr_3LaCuRuO_8$, $Sr_{3.5}La_{0.5}CuRuO_{8-\delta}$, $Sr_3LaZnRuO_8$, $Sr_2LaCuRuO_{7-\delta}$, and $Sr_{2.15}La_{0.85}CuRuO_{7-\delta}$. There is no evidence for the presence of Cu^{3+} in any of these samples. The electrical conductivities of these phases, and also those of $Sr_{1.2}La_{0.8}CuRuO_{6-\delta}$ and $Sr_2LaZnRuO_7$, have been measured as a function of temperature. All these materials are semiconductors, but none shows long range magnetic order at 1.5 K.

Introduction

There are two extreme descriptions of the valence shell d electrons on a transition metal cation in a mixed metal oxide. If the interatomic electron–electron interactions are much stronger than those between electrons on the same cation, then the d electrons are delocalized and the properties of the compound are best described by band theory. However, if the intra-atomic interactions are dominant, we expect the electrons to be localized. In the latter case, the compound is likely to be an electrical insulator and to show long-range magnetic order at low temperatures. At higher temperatures the magnetic susceptibility of such a material is expected to follow the Curie–Weiss Law, whereas that of a delocalized system will exhibit Pauli Paramagnetism at all temperatures. Oxides containing the cation Ru(V) are of particular interest to us, because they often show electronic properties which suggest that neither extreme description is appropriate to them, the behavior of the $4d^3$ valence electron configuration being intermediate in character. This has been demonstrated in a number of compounds; for example, the perovskite Ba_2LaRuO_6 orders antiferromagnetically with $T_N = 30$ K (*1*), but the value of ca. 4.1 μ_B measured for the effective magnetic moment in the paramagnetic phase is significantly greater than the maximum value allowed by the localized electron model ($\mu_{S.O.} = 3.87\ \mu_B$). This behavior suggests that the degree of covalency in the Ru(V)–O bonds is large enough to give the d bands a significant

* To whom correspondence should be addressed.

0022-4596/92 $3.00

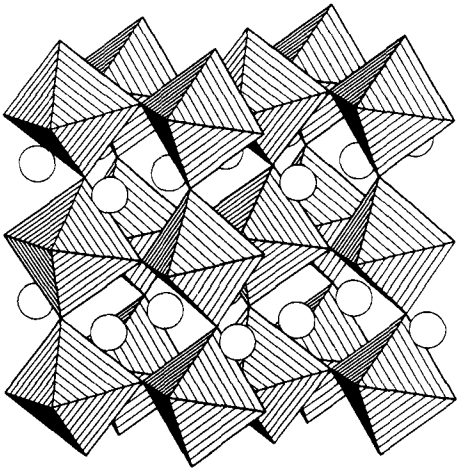

FIG. 1. The perovskite structure of ABO_3 shown as a network of BO_6 octahedra with A cations occupying holes in the framework. The structure is drawn with orthorhombic symmetry.

width, and that it may be possible to prepare mixed metal oxides of Ru(V) which show metallic conductivity. However, in order to achieve this goal it will be necessary to overcome the particularly large correlation energy associated with the t_{2g}^3 electron configuration of 6-coordinate Ru(V).

The discovery of high electrical conductivities in many mixed valence, perovskite-related oxides of copper prompted us to prepare and characterize a number of mixed Cu/Ru oxides in which it is possible to envisage an interaction between the partially filled e_g^* band of Cu^{2+} and the broad, empty e_g^* band of Ru(V). We attempted to introduce this pair of cations into the perovskite structure (Fig. 1), the Ruddlesden–Popper structure (Fig. 2), and the K_2NiF_4 structure (Fig. 3) so as to monitor the change in electrical properties with the decreasing dimensionality (from 3-D to 2-D) of the crystal structure. The compositions chosen for study included some in which the cations were expected to be in an integral oxidation state and others in which we hoped to find mixed valency. More specifically, we prepared the perovskites $SrLaCuRuO_6$ and $Sr_{1.2}La_{0.8}CuRuO_6$, the latter in the hope that we might introduce extra holes into the copper $3d$-band and thus induce a high electrical conductivity. Similarly, we synthesized the K_2NiF_4 phases $Sr_3LaCuRuO_8$, $Sr_{3.5}La_{0.5}CuRuO_8$, and, in order to monitor the effect of unit cell size, $Sr_3NdCuRuO_8$. In the Ruddlesden–Popper structural family (*2*) we made $Sr_2LaCuRuO_7$ and $Sr_{2.15}La_{0.85}CuRuO_7$. Finally, in order to provide a comparison between the behavior of transition metal cations and that of isovalent main-group ions, we also prepared $SrLaCuSbO_6$, $Sr_3LaZnRuO_8$, and $Sr_2LaZnRuO_7$. In this paper we describe the synthesis conditions used to prepare these compounds, the behavior of their electrical conductivities as a function of temperature, and, for a selected

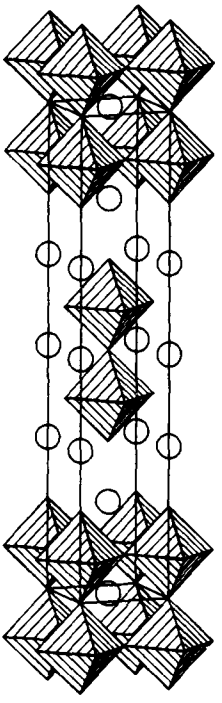

FIG. 2. The Ruddlesden–Popper ($A_3B_2O_7$) structure consisting of separated double layers of BO_6 octahedra with A cations occupying holes in the framework and in the interlayer spacing.

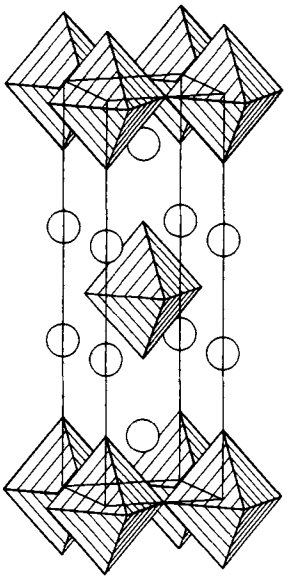

FIG. 3. The K_2NiF_4 (or A_2BO_4) structure consisting of separated layers of BO_6 octahedra with A cations occupying holes in the interlayer spacing.

subset of the materials, the results of crystal structure refinements carried out by neutron powder diffraction.

Experimental

Polycrystalline samples of the mixed metal oxides listed in Table I were prepared by firing the appropriate stoichiometric quantities of dry $SrCO_3$, La_2O_3, Nd_2O_3, RuO_2, CuO, ZnO, and Sb_2O_3 in air at the tabulated temperatures. The reaction mixtures were pelletized and contained in alumina crucibles during the syntheses, each of which lasted for several days and involved repeated grinding and reforming of the pellets. The reactions were judged to be complete when the room temperature X-ray diffraction patterns of the products were constant. The final cooling of the product simply involved removing the crucible from the furnace at the firing temperature and allowing it to cool slowly to room temperature in air. Neutron powder diffraction data were collected on seven samples at either room temperature or 1.5 K, as detailed below. The diffractometer D1a at ILL Grenoble was used with a mean neutron wavelength of 1.9127, 1.9080, or 1.9116 Å. In all cases the samples were contained in vanadium cans and data were collected at 2θ intervals of 0.05° in the range $0 \leq 2\theta \leq 160°$. The crystal structures were refined using the Brookhaven version (*3*) of the Rietveld (*4*) program. The peaks were fitted by a pseudo-Voigt function with a correction made to model the asymmetry of the low-angle peaks. The background level was estimated by interpolation between regions of the profile where there were no Bragg peaks. Electrical conductivity measurements were made by using a 4-probe dc technique. Colloidal silver paint was used to attach metallic contacts to small, well-sintered ingots of the samples (ca. 1.5 × 1.5 × 8 mm), which were mounted in an Oxford Instruments cryostat for measurements in the temperature range $80 \leq T \leq 300$ K. The two current contacts were attached to the ends of the bar, and the two voltage contacts were made near its center, with a separation of ~2.5 mm.

Results

1. Synthesis and Structural Characterization

(a) The perovskites $SrLaCuRuO_6$, $Sr_{1.2}La_{0.8}CuRuO_6$ and $SrLaCuSbO_6$. The room temperature X-ray powder diffraction pattern of $SrLaCuRuO_6$ indicated that this compound has a distorted perovskite-like structure (Fig. 1), similar to that reported previously for La_2NiRuO_6 (*5*). It was not possible to derive accurate unit cell parameters from our powder pattern, and in Table I we therefore give an approximate pseudocubic value. A full structural study by neutron diffraction was carried out at a temperature of 1.5 K (λ = 1.9127 Å). Our initial

TABLE I

EXPERIMENTAL CONDITIONS AND ROOM TEMPERATURE UNIT CELL PARAMETERS

Compound	Firing temperature (K)	a (Å)	c (Å)
$SrLaCuRuO_6$	1423	7.87_6[a]	
$Sr_{1.2}La_{0.8}CuRuO_6$	1423	7.87_4[a]	
$SrLaCuSbO_6$	1473	5.51[b]	8.39[b]
$Sr_3NdCuRuO_8$	1423	3.8733(7)	12.711(2)
$Sr_3LaCuRuO_8$	1423	3.900(1)	12.725(4)
$Sr_{3.5}La_{0.5}CuRuO_{8-\delta}$	1423	3.8996(7)	12.613(2)
$Sr_3LaZnRuO_8$	1373	3.9348(9)	12.654(3)
$Sr_2LaCuRuO_7$	1423	3.919(1)	20.460(7)
$Sr_{2.15}La_{0.85}CuRuO_{7-\delta}$	1373	3.924(1)	20.300(6)
$Sr_2LaZnRuO_7$	1373	3.962(2)	20.40(2)

[a] Pseudo-cubic unit cell parameter for an orthorhombic compound.
[b] Pseudo-tetragonal unit cell parameters for a monoclinic compound.

refinements indicated that the compound was indeed a distorted perovskite with a disordered arrangement of Sr and La over the *A* sites and a disordered distribution of Cu and Ru over the 6-coordinate *B* sites. We were thus led to assign the structure to the orthorhombic spacegroup *Pbnm*. Subsequent refinement of 11 structural parameters and the appropriate profile parameters resulted in values of 6.8 and 4.1% for the weighted-profile (R_{wpr}) and intensity (R_I) *R* factors. The final atomic parameters are listed in Table II, and the corresponding bond lengths and bond angles are given in Table III. The standard deviations quoted with the structural parameters in this paper are those produced by the Rietveld program, and they thus indicate the precision of the refined parameters; the accuracy of the bond lengths is likely to be limited by the accuracy of the wavelength calibration, which we estimate to be ±0.001 Å. The final observed and calculated diffraction patterns are drawn in Fig. 4. We were able to prepare Sr-rich samples of this phase up to the composition $Sr_{1.2}La_{0.8}CuRuO_6$. These samples were not studied by neutron diffraction, but the room temperature unit cell parameter of the end member is given in Table I. Photoelectron spectroscopy (*6*) showed that copper was predominantly present as Cu^{2+} in all the compounds described in this paper, an observation which implies that oxygen vacancies were introduced on doping with excess strontium.

The X-ray powder diffraction pattern of $SrLaCuSbO_6$ was very different in appearance to that of the Ru analogue. The Sb compound has been reported previously (*7*) as a tetragonal perovskite, but our data showed additional splittings on some Bragg peaks that could only be explained by assuming that the symmetry was monoclinic. Neutron diffraction data collected at room temperature (λ = 1.9116 Å) were consistent with the lowering of the symmetry to space group $P2_1/n$. This space group allows two crystallographically distinct sites for the 6-coordinate cations in the perovskite structure, and our final refinements were thus carried out with a disordered arrangement of Sr and La, as in $SrLaCuRuO_6$, but with an ordered 1 : 1 arrangement of Cu and Sb over the octahedral sites. Refinement of 18 atomic parameters and the usual profile parameters converged with R_{wpr} = 4.4%. The final structural parameters are listed in Table IV, and the bond lengths and bond angles are given in Table V.

TABLE II

STRUCTURAL PARAMETERS FOR $SrLaCuRuO_6$ AT 1.5 K (SPACE GROUP *Pbnm*)

Atom	Site	x	y	z	B_{iso} (Å^2)
Sr/La	4*c*	0.0038(4)	0.0242(3)	$\frac{1}{4}$	0.89(3)
Cu/Ru	4*b*	$\frac{1}{2}$	0	0	0.52(3)
O1	8*d*	0.2783(4)	0.2757(4)	0.0333(2)	1.71(3)
O2	4*c*	−0.0674(5)	0.4945(5)	$\frac{1}{4}$	1.35(5)

Note. a = 5.6041(3), b = 5.5810(3), c = 7.8489(4) Å; R_I = 4.1, R_{wpr} = 6.8%.

Figure 5 shows the final observed and calculated diffraction patterns.

(*b*) *The Ruddlesden–Popper phases* $Sr_2LaCuRuO_7$, $Sr_{2.15}La_{0.85}CuRuO_7$, *and* $Sr_2LaZnRuO_7$. The room temperature X-ray diffraction patterns of the Cu compounds could be indexed in the tetragonal space group *I*4/*mmm* (Table I) with unit cell parameters consistent with the adoption of a Ruddlesden–Popper structure. Neutron diffraction data collected at 1.5 K using wavelengths of λ = 1.9116 Å ($Sr_2LaCuRuO_7$) and λ = 1.9080 Å ($Sr_{2.15}La_{0.85}CuRuO_7$) showed no evidence of any distortion to a lower symmetry, and refinement of the structures led to the atomic coordinates, occupation factors, and anisotropic temperature factors presented in Table VI, the corresponding bond lengths being listed in Table VII. Atom O1 is the oxide ion at the center of the perovskite-like slab (Fig. 2), O2 forms a pseudo-*xy* plane with the transition metal cations, and O3 lies on the edges of the slabs. Similarly, Sr/La1 lies between the slabs, whereas Sr/La2 lies within them. We felt it was inappropriate to use isotropic temperature factors to describe a structure with a marked 2-dimensional character. Vacancies were introduced onto the oxygen sites in response to the high values of their temperature factors. The site O1 (but not O2) showed a significant vacancy concentration in both compounds, and their formulae are henceforth modified to reflect this. Again we found no evidence for cation ordering on the Cu/Ru or Sr/La sublattices, even though there are two crystallographically distinct sites for the larger cations in this structure. The observed and calculated diffraction patterns of $Sr_2LaCuRuO_{7-\delta}$ are shown in Fig. 6; the corresponding diagram for $Sr_{2.15}La_{0.85}CuRuO_{7-\delta}$ is essentially identical. $Sr_2LaZnRuO_7$ was not studied by neutron diffraction. The X-ray pattern was essentially that of a Ruddlesden–Popper phase, although there was some evidence for a slight orthorhombic distortion of the unit cell.

TABLE III

BOND LENGTHS (IN Å) AND BOND ANGLES (IN DEGREES) FOR $SrLaCuRuO_6$ AT 1.5 K

Distances			
Sr/La–O1		Sr/La–O2	
2.689(5)	(×2)	2.983(5)	
2.790(5)	(×2)	2.655(5)	
2.512(5)	(×2)	2.451(5)	
Cu/Ru–O1		Cu/Ru–O2	
1.995(4)	(×2)	1.998(4)	(×2)
2.017(4)	(×2)		
mean Sr/La–O: 2.675			
mean Cu/Ru–O: 2.003			
shortest O–O contact: O1–O1′ 2.808(5)			
Angles			
O1–Cu/Ru–O1 91.13			
O1–Cu/Ru–O2 90.06			
Cu/Ru–O1–Cu/Ru 160.6			
Cu/Ru–O2–Cu/Ru 158.2			

(*c*) *The* K_2NiF_4 *phases* $Sr_3NdCuRuO_8$,

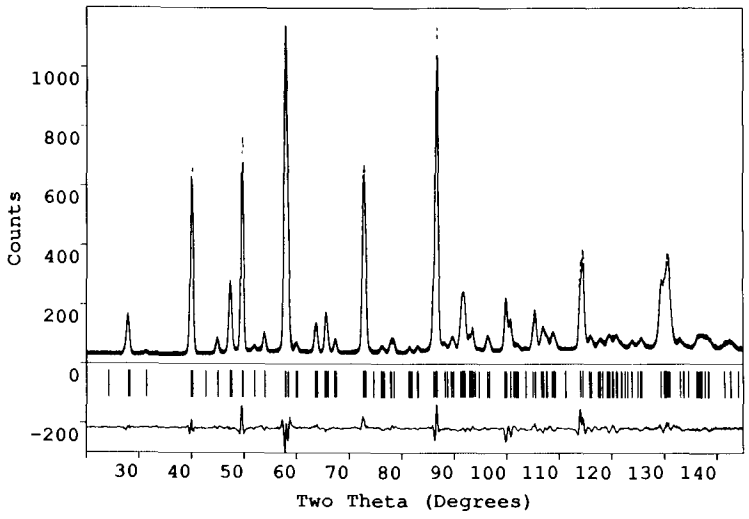

FIG. 4. The observed (·····), calculated (-), and difference neutron powder diffraction profiles of $SrLaCuRuO_6$ at 1.5 K. Reflection positions are marked.

$Sr_3LaCuRuO_8$, $Sr_{3.5}La_{0.5}CuRuO_8$, and $Sr_3LaZnRuO_8$. The X-ray diffraction patterns of all these products could be indexed in a body-centered tetragonal unit cell of size ca. 3.9 × 3.9 × 12.6 Å, consistent with the adoption of a K_2NiF_4 structure with no ordering of the Sr/Ln or Cu/Ru cations (Table I). Neutron diffraction data were collected at a temperature of 1.5 K using a wavelength of 1.9127 Å (1.9116 Å for Nd). Refinement of the structure of the Nd compound proceeded smoothly in space group *I4/mmm* to give the structural parameters listed in Table VIII and the profiles drawn in Fig. 7. Anisotropic temperature factors were used for all atoms. The analysis of the structure of $Sr_3LaCuRuO_8$ is the least satisfactory of those described in this paper. The profile plots in Fig. 8 and the relative values of R_{wpr} and R_T (Table VIII) suggest that this is in part due to an inadequate description of the peak shape rather than to inadequacies in the structural model. It became clear during the study of the Sr-rich sample $Sr_{3.5}La_{0.5}CuRuO_8$ that our attempt to introduce Cu^{3+} had largely failed and that the deficit of positive charge was balanced by the presence of vacancies on the anion sublattice. As can be seen from Fig. 3, there are two oxygen sites in this structure which are clearly "chemically" distinct, as well as being crystallographically inequivalent. One of these (O2) lies in the center of the perovskite-like layers, the other (O1) lies on the edge of the layers. Our refinements showed that the vacancies were confined to

TABLE IV

STRUCTURAL PARAMETERS FOR $SrLaCuSbO_6$ AT ROOM TEMPERATURE (SPACE GROUP $P2_1/n$)

Atom	Site	x	y	z	B_{iso} (Å^2)
Sr/La	4*e*	0.0107(2)	0.0232(2)	0.2485(1)	0.69(2)
Cu	2*e*	½	0	½	0.61(2)
Sb	2*d*	½	0	0	0.21(3)
O1	4*e*	0.2833(3)	0.2810(3)	0.0390(2)	1.01(3)
O2	4*e*	0.2190(3)	−0.2181(3)	0.0376(2)	0.87(3)
O3	4*e*	−0.0680(2)	0.4918(3)	0.2709(2)	0.96(2)

Note. a = 5.5295(1), b = 5.5243(1), c = 8.4190(1) Å; β = 90.49(1)°; R_I = 2.9, R_{wpr} = 4.4%.

TABLE V

BOND LENGTHS (IN Å) AND BOND ANGLES (IN DEGREES) FOR $SrLaCuSbO_6$ AT ROOM TEMPERATURE

Distances		
Sr/La–O1	Sr/La–O2	Sr/La–O3
2.731(4)	2.508(4)	2.974(4)
2.501(4)	2.920(4)	2.632(4)
2.964(4)	2.733(4)	2.458(4)
Cu–O1	Cu–O2	Cu–O3
2.004(3) (×2)	1.996(3) (×2)	2.315(3) (×2)
Sb–O1	Sb–O2	Sb–O3
1.990(3) (×2)	1.994(3) (×2)	1.963(3) (×2)

mean Sr/La–O = 2.713
mean Cu–O = 2.105
mean Sb–O = 1.982

shortest O–O contact: O1–O3, 2.748(4)

Angles			
O1–Cu–O2	91.56	O1–Sb–O2	91.49
O1–Cu–O3	92.28	O1–Sb–O3	91.92
O2–Cu–O3	92.16	O2–Sb–O3	91.55
Cu–O1–Sb	156.2	Cu–O2–Sb	156.7
Cu–O3–Sb	159.5		

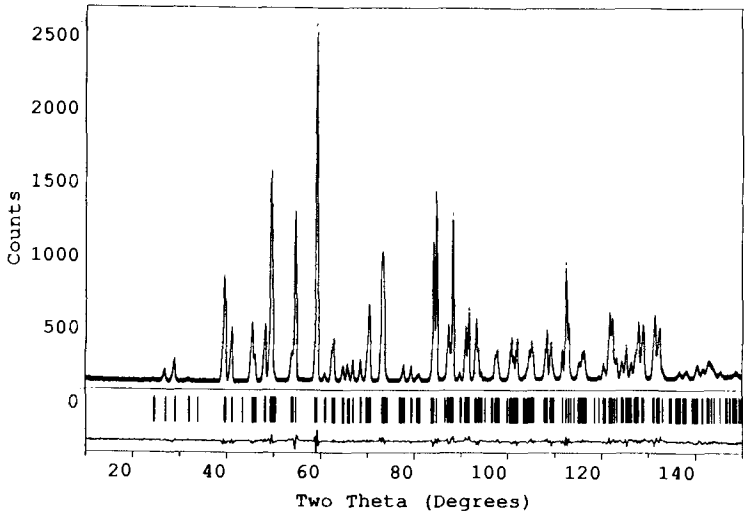

FIG. 5. The observed (·····), calculated (-), and difference neutron powder diffraction profiles of $SrLaCuSbO_6$ at room temperature. Reflection positions are marked.

TABLE VI

STRUCTURAL PARAMETERS FOR $Sr_2LaCuRuO_{7-\delta}$ AND $Sr_{2.15}La_{0.85}CuRuO_{7-\delta}$ AT 1.5 K (SPACE GROUP *I4/mmm*)

Atom	Parameter	Compound	
		$Sr_2LaCuRuO_{7-\delta}$	$Sr_{2.15}La_{0.85}CuRuO_{7-\delta}$
Sr/La1	z	0.31741(4)	0.31735(6)
	B_{11}(Å^2)	0.73(3)	0.79(4)
	B_{33}	0.42(5)	0.52(7)
Sr/La2	B_{11}	0.46(3)	0.54(5)
	B_{33}	0.40(7)	0.4(1)
Cu/Ru	z	0.09738(5)	0.09752(7)
	B_{11}	0.22(2)	0.15(3)
	B_{33}	0.81(4)	0.67(6)
O1	B_{11}	4.01(9)	3.8(1)
	B_{33}	1.3(1)	0.8(2)
	N^a	0.898(5)	0.907(5)
O2	z	0.09507(5)	0.09498(6)
	B_{11}	0.88(3)	0.95(5)
	B_{22}	0.51(3)	0.56(5)
	B_{33}	3.59(4)	3.28(7)
O3	z	0.19919(7)	0.1983(1)
	B_{11}	2.23(4)	2.01(5)
	B_{33}	1.34(8)	1.2(1)
	a (Å)	3.91958(5)	3.92062(8)
	c (Å)	20.4529(3)	20.3006(4)
	V (Å^3)	314.22(1)	312.04(1)
	R_I	1.97	2.31
	R_{wpr}	4.08	5.46

Note. Sr/La1, Cu/Ru, and O3 on 4*e*; Sr/La2 on 2*b*; O1 on 2*a*; O2 on 8*g*.

[a] Occupation factor for site O1.

the O2 sublattice. In order to confirm this conclusion we collected a second data set on the same sample at room temperature; the occupation factor for site O2 then refined to a value of 0.926(4), not significantly different from the value of 0.929(4) found at 1.5 K. The final low-temperature profiles for $Sr_{3.5}La_{0.5}CuRuO_{8-\delta}$ are plotted in Fig. 9. The neutron diffraction data collected on $Sr_3LaZnRuO_8$ showed a number of weak peaks which were not seen in the X-ray diffraction pattern collected at room temperature. This small impurity content did not hinder the refinement of the crystal structure of the principal phase, the results of which are given in Table VIII. The peaks arising from the second phase are visible in the observed diffraction profile drawn as part of Fig. 10. The most important bond lengths found in the compounds discussed in this section are compared in Table IX.

II. Electrical Measurements

The resistivities of the compounds under discussion, with the exception of $SrLaCuSbO_6$, are plotted as a function of temperature in Fig. 11. All of the data are consistent with semiconducting, rather than metallic, behavior. Attempts to account for the observed temperature dependence in terms of an Arrhenius-type model for conductivity were unsuccessful, as were those based on a polaronic model. However, excellent agreement between theory and experiment was obtained when the Mott Variable Range Hopping (VRH) model (*8*) was used. Least-squares fitting of the resistivity data to the expression (*9*)

$$\rho = \rho_0(T/T_0)^{1/2}\exp[(T_0/T)^{\omega}]$$

gave $\omega = 0.25 + 0.01$ for all samples. A

TABLE VII

BOND LENGTHS IN (Å) FOR $Sr_2LaCuRuO_{7-\delta}$ AND $Sr_{2.15}La_{0.85}CuRuO_{7-\delta}$ AT 1.5 K

Bond		Compound	
		$Sr_2LaCuRuO_{7-\delta}$	$Sr_{2.15}La_{0.85}CuRuO_{7-\delta}$
Cu/Ru–O1		1.992(1)	1.980(1)
Cu/Ru–O2	(×4)	1.960(1)	1.961(1)
Cu/Ru–O3		2.082(1)	2.046(1)
mean Cu/Ru–O		1.986	1.978
Sr/La1–O2	(×4)	2.654(1)	2.648(1)
Sr/La1–O3		2.418(1)	2.417(1)
Sr/La1–O3′	(×4)	2.792(1)	2.790(1)
Sr/La2–O1	(×4)	2.772(1)	2.772(1)
Sr/La2–O2	(×8)	2.761(1)	2.750(1)
mean Sr/La–O		2.732	2.726
shortest O–O contact		2.761	2.750

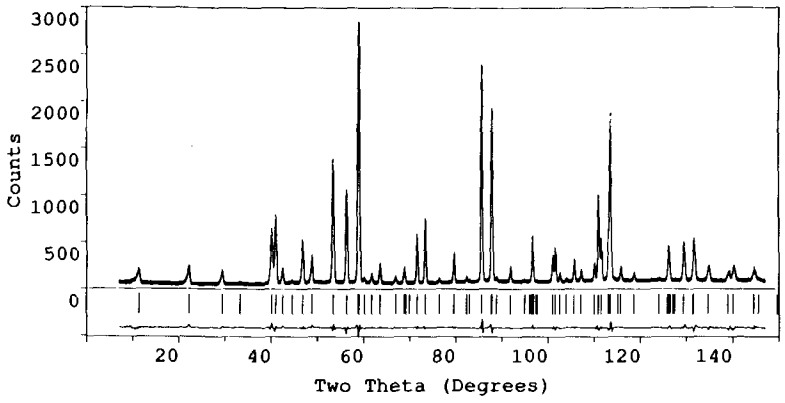

FIG. 6. The observed (·····), calculated (-), and difference neutron powder diffraction profiles of $Sr_2LaCuRuO_7$ at 1.5 K. Reflection positions are marked.

TABLE VIII

STRUCTURAL PARAMETERS FOR $Sr_3NdCuRuO_8$, $Sr_3LaCuRuO_8$, $Sr_{3.5}La_{0.5}CuRuO_{8-\delta}$, AND $Sr_3LaZnRuO_8$ AT 1.5 K

		Compound			
Atom	Parameter	$Sr_3NdCuRuO_8$	$Sr_3LaCuRuO_8$	$Sr_{3.5}La_{0.5}CuRuO_{8-\delta}$	$Sr_3LaZnRuO_8$
Sr/Ln	z	0.35594(9)	0.3564(2)	0.35568(8)	0.3576(1)
	B_{11} (Å^2)	0.58(4)	0.55(4)	0.60(3)	0.17(3)
	B_{33}	0.73(6)	0.5(1)	0.28(6)	0.74(7)
Cu/Ru	B_{11}	0.29(3)	0.25(6)	0.57(4)	0.07(6)
(or Zn)	B_{33}	0.29(6)	1.3(2)	0.27(8)	0.4(1)
O1	z	0.1658(1)	0.1641(2)	0.1617(1)	0.1653(2)
	B_{11}	1.57(3)	1.20(6)	1.08(3)	1.11(4)
	B_{33}	1.34(8)	1.1(2)	0.73(8)	0.4(1)
O2	B_{11}	0.44(5)	0.4(1)	0.56(6)[a]	0.05(7)
	B_{22}	1.41(5)	1.6(1)	1.52(6)	0.59(7)
	B_{33}	0.60(7)	0.8(1)	0.45(7)	0.50(9)
	a (Å)	3.86413(7)	3.8869(1)	3.88886(8)	3.9247(1)
	c (Å)	12.6951(2)	12.7082(5)	12.5986(2)	12.6288(4)
	V (Å^3)	189.56(1)	191.99(2)	190.53(1)	194.52(2)
	R_I (%)	2.7	3.6	2.2	2.8
	R_{wpr} (%)	5.1	10.6	4.9	7.22

Space group $I4/mmm$: Sr/La or Sr/Nd on 4e (00z)
Cu/Ru or Zn/Ru on 2a (000)
O1 on 4e (00z)
O2 on 4c ($\frac{1}{2}$00)

[a] Occupation factor for site O2 in $Sr_{3.5}La_{0.5}CuRuO_{8-\delta}$ is 0.929(4).

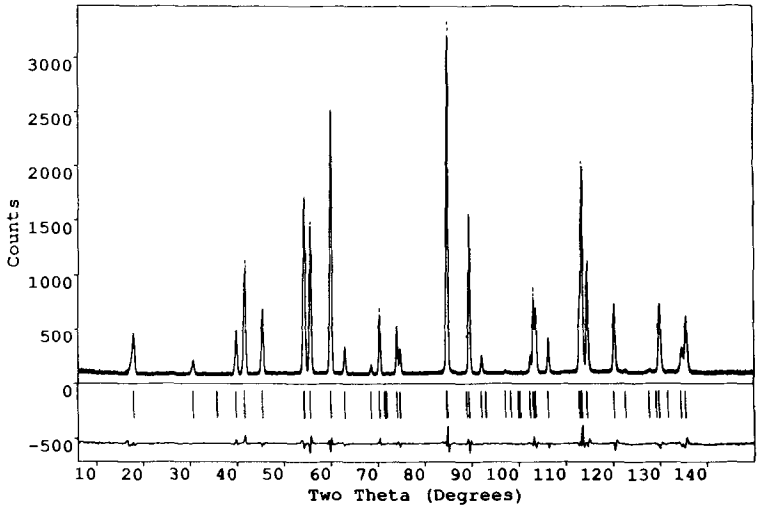

FIG. 7. The observed (·····), calculated (-), and difference neutron powder diffraction profiles of $Sr_3NdCuRuO_8$ at 1.5 K. Reflection positions are marked.

value of $\frac{1}{4}$ is expected for conduction by 3-dimensional VRH ($\frac{1}{3}$ for 2-D). However, it must be remembered that our measurements were made on samples which were polycrystalline, albeit well sintered, and our data will therefore contain a contribution from the conductivity of the grain boundaries. We were unable to make the thermopower measurements that would have enabled us to eliminate this effect, and the validity of the VRH model is therefore not proven. The room temperature resistivity of

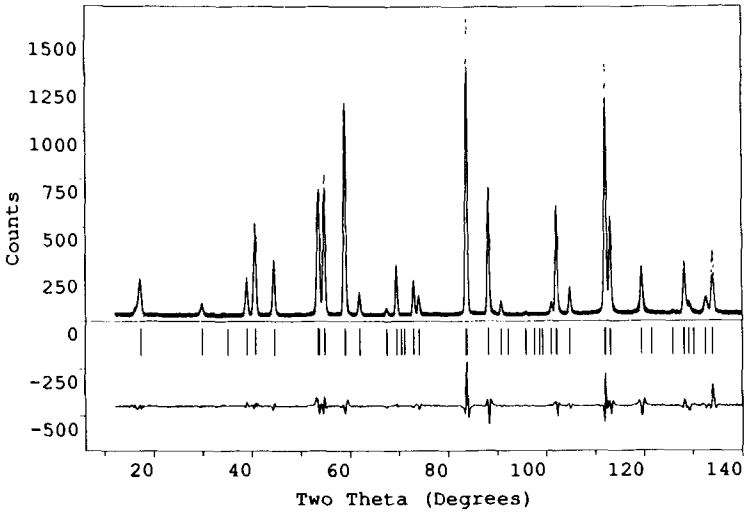

FIG. 8. The observed (·····), calculated (-), and difference neutron powder diffraction profiles of $Sr_3LaCuRuO_8$ at 1.5 K. Reflection positions are marked.

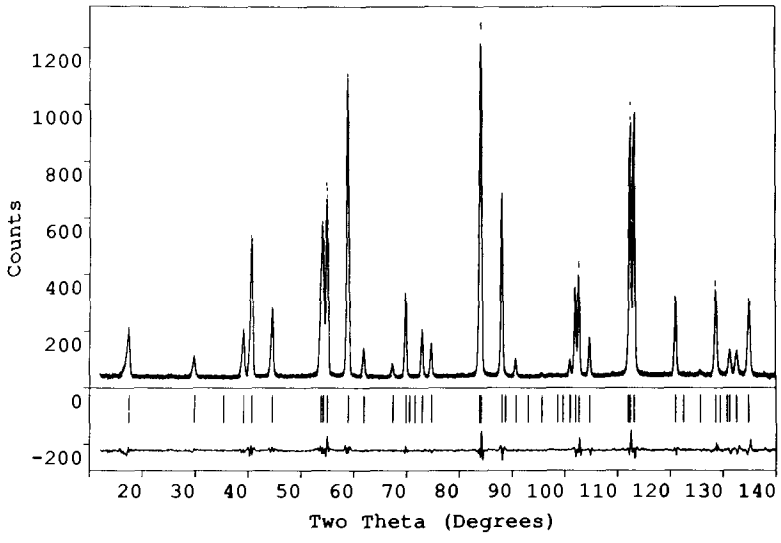

FIG. 9. The observed (·····), calculated (-), and difference neutron powder diffraction profiles of $Sr_{3.5}La_{0.5}CuRuO_{8-\delta}$ at 1.5 K. Reflection positions are marked.

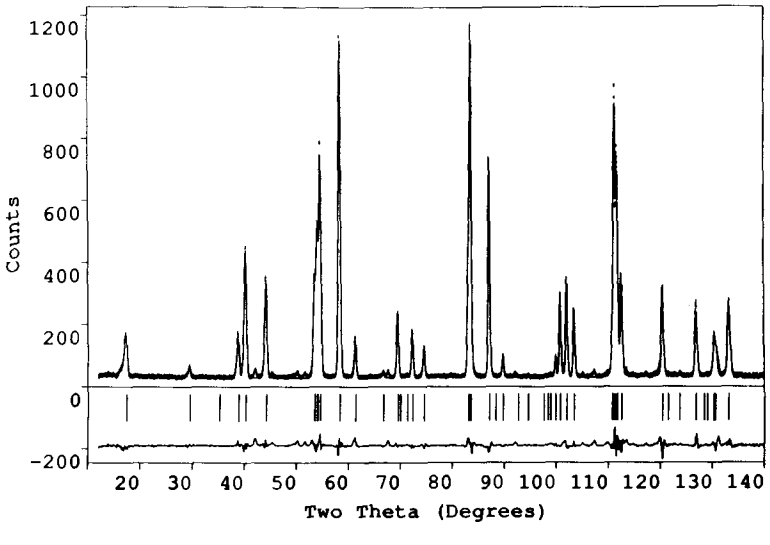

FIG. 10. The observed (·····), calculated (-), and difference neutron powder diffraction profiles of $Sr_3LaZnRuO_8$ at 1.5 K. Reflection positions are marked.

TABLE IX

BOND LENGTHS (IN Å) FOR $Sr_3NdCuRuO_8$, $Sr_3LaCuRuO_8$, $Sr_{3.5}La_{0.5}CuRuO_{8-\delta}$, AND $Sr_3LaZnRuO_8$ AT 1.5 K

Bond	Compound			
	$Sr_3NdCuRuO_8$	$Sr_3LaCuRuO_8$	$Sr_{3.5}La_{0.5}CuRuO_{8-\delta}$	$Sr_3LaZnRuO_8$
Cu/Ru–O1 (×2)	2.104(3)	2.072(3)	2.038(3)	2.087(3)
Cu/Ru–O2 (×4)	1.932	1.943	1.944	1.962
mean Cu/Ru–O	1.989	1.986	1.975	2.004
Sr/Ln–O1	2.414(4)	2.457(4)	2.443(4)	2.429(4)
Sr/Ln–O1 (×4)	2.746(4)	2.760(4)	2.759(4)	2.790(4)
Sr/Ln–O2 (×4)	2.660(3)	2.666(3)	2.662(3)	2.662(3)
mean Sr/Ln–O	2.671	2.685	2.681	2.693

$SrLaCuSbO_6$ was so large ($> 10^6\ \Omega$ cm) that we did not continue the experiment to low temperatures.

Discussion

In view of the nonmetallic conductivity behavior described above, the crystal structure data is discussed in terms of a localized electron model but with the $Cu^{2+}: 3d^9$ and $Ru^{5+}: 4d^3$ energy levels assumed to have a finite width.

The crystal structure of $SrLaCuRuO_6$ is that of a simple orthorhombic perovskite with disorder present on both the *A* and the *B* sublattices. Many perovskite-related

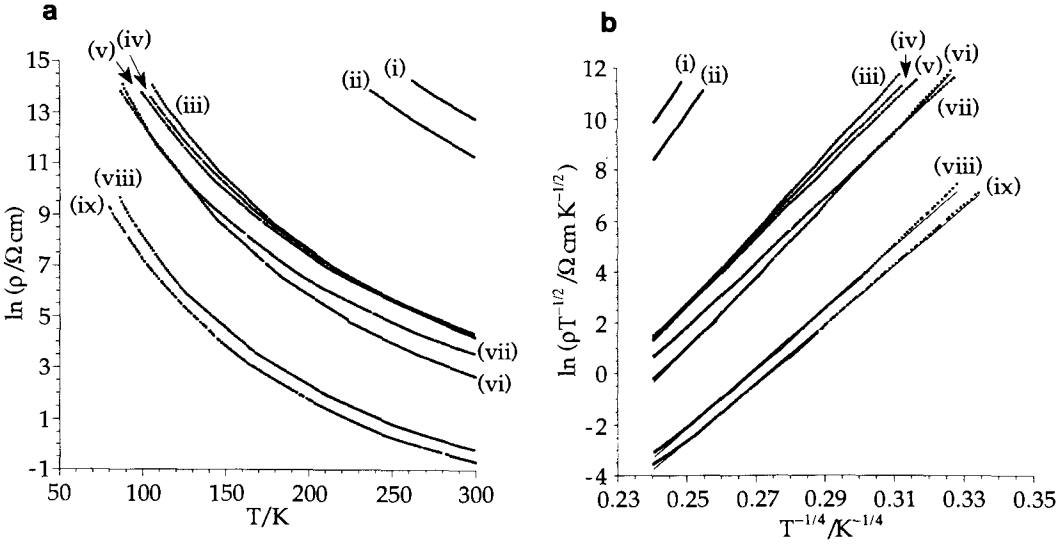

FIG. 11. The resistivity of mixed oxides of Ru and Cu as a function of temperature: (i) $Sr_3LaZnRuO_8$; (ii) $Sr_2LaZnRuO_7$; (iii) $Sr_{2.15}La_{0.85}CuRuO_{7-\delta}$; (iv) $Sr_{3.5}La_{0.5}CuRuO_{8-\delta}$; (v) $Sr_3LaCuRuO_8$; (vi) $Sr_2LaCuRuO_{7-\delta}$; (vii) $Sr_3NdCuRuO_8$; (viii) $SrLaCuRuO_6$; and (ix) $Sr_{1.2}La_{0.8}CuRuO_6$.

materials have a mixture of Sr^{2+} and La^{3+} on the *A* sites (*10*), and in the majority of cases there is no long-range ordering of the two cation species. Ordering of two different cations over the *B* sites is more common (*11*), although we have previously shown that Ru^{5+} forms disordered arrays with both Ni^{2+} and Zn^{2+} (*12*) and so the disorder observed in $SrLaCuRuO_6$ is perhaps not surprising. The Cu/Ru–O bond lengths listed in Table III are very similar to those reported previously (*12*) for the Ni/Ru–O and Zn/Ru–O bonds in $BaLaNiRuO_6$ and $BaLaZnRuO_6$, respectively. However, there is a difference between $SrLaCuRuO_6$ and the other compounds in that the electron distributions around Ru^{5+}, Ni^{2+}, and Zn^{2+} are expected to be spherical when the cations are in octahedral coordination, whereas that around Cu^{2+} is not. The environment around the latter would normally be expected to undergo a Jahn–Teller distortion, and $SrLaCuRuO_6$ thus contains two transition metal ions with different coordination preferences. The observed disorder is therefore more noteworthy than previously suggested. The isotropic temperature factors of the oxide ions O1 and O2 are too high (Table II) to simply represent the thermal motion of these atoms at a temperature of 1.5 K. Attempts to eliminate the high-temperature factors by introducing anion vacancies were unsuccessful in this case, and we believe that it is likely that the disorder causes local displacements of the anions from their mean positions, the magnitude of these displacements being determined by the local disposition of Sr/La and Cu/Ru about the oxide ion. The tendency of Cu^{2+} to occupy a tetragonally distorted, 6-coordinate site is manifest in the crystal structure of SrLa $CuSbO_6$ (Fig. 12). This differs markedly from that of $SrLaCuRuO_6$ in that the Cu^{2+} and Sb^{5+} cations form a 1 : 1 ordered array, the SbO_6 octahedra being approximately regular whereas the CuO_6 octahedra have a *c*/*a* ratio of 1.15. It is not clear why the

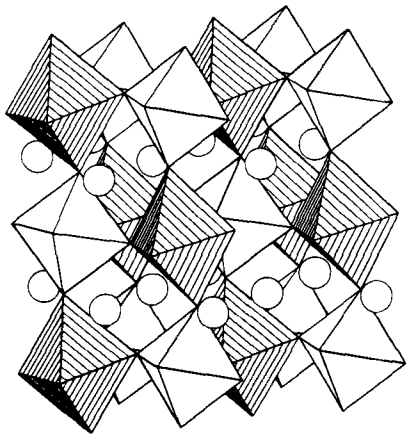

FIG. 12. The monoclinic crystal structure of the ordered perovskite $SrLaCuSbO_6$. CuO_6 octahedra are shaded, SbO_6 octahedra are unshaded.

Sb-containing compound adopts an ordered cation arrangement when the Ru analogue does not. The occurrence of long-range cation ordering in this type of compound is usually thought to depend on the difference in the size and charge of the two species involved. The nominal charge difference is the same in these two compounds, and the size difference is less in the case of the ordered Sb compound. It is therefore necessary to consider other factors, for example cation polarizability, in order to explain our observations. The isotropic temperature factors of the oxide ions in $SrLaCuSbO_6$ are lower at room temperature than those determined for $SrLaCuRuO_6$ at 1.5 K. This is presumably because the long-range order over the *B* sites in the former compound largely eliminates the local distortions referred to above, despite the residual disorder on the Sr/La sublattice.

There is no long-range order between Cu and Ru in the Ruddlesden–Popper phases described in Tables VI and VII, and the temperature factors of the oxide ions are again large enough to imply that the ions are displaced from their ideal positions in the crystal structure. The interpretation of the

structural data is made more difficult by the need to include in the model a 10% vacancy concentration on the anion site at the center of the perovskite slab (O1). The average transition metal environment in $Sr_2LaCuRuO_{7-\delta}$ has a marked asymmetry, with the Cu/Ru–O1 distance being 0.09 Å shorter than the other axial bond length, Cu/Ru–O3. A distortion of this magnitude is consistent with the presence of Cu^{2+}, and hence incomplete oxidation of Ru(IV) to Ru(V) during synthesis is implied in order to account for the oxygen stoichiometry. The oxygen content is essentially unchanged in the Sr-rich sample, implying that more extensive oxidation of the Ru has taken place. This model would account for the existence of Sr-rich compositions up to $Sr_{2.2}La_{0.8}CuRuO_{6.9}$; any increase in Sr content beyond this level would require the oxidation of Cu^{2+} or an increase in the anion vacancy concentration. The observation of a smaller, less asymmetric Cu/Ru site in the doped compound is consistent with the replacement of Ru(IV) by Ru(V). However, more samples with different Sr/La ratios must be made and characterised if an unambiguous model is to be deduced for these Ruddlesden–Popper compounds. A study of the local cation environments by EXAFS might be beneficial.

It is convenient to discuss the structural results described above for the K_2NiF_4 phases in the sequence of presentation used in Tables VIII and IX. $Sr_3NdCuRuO_8$ and $Sr_3LaCuRuO_8$ differ only in the size of the rare earth cations, which occupy 25% of the 9-coordinate sites (Fig. 3). Predictably, the unit cell parameters increase on moving from the Nd compound to the La analogue. More interestingly, the c/a ratio of the Cu/Ru–O_6 octahedra decreases from 1.089 to 1.066, although the mean Cu/Ru–O bond length remains virtually unchanged. The increase in length of the equatorial Cu/Ru–O bonds is imposed by the marked increase in size of the *ab* plane of the unit cell, which is in turn caused by the replacement of Nd^{3+} by the larger La^{3+}. In order to conserve the total bond strength around Cu/Ru, the axial Cu/Ru–O bonds are shortened, thus producing the required lengthening of the axial Ln–O1 bond. This interpretation of the observations implies that this structure has the freedom to adapt along the c axis, while being strained in the *ab* plane; the extent to which the Cu/Ru–O2 bonds are compressed in $Sr_3NdCuRuO_8$ can be seen by comparing the data in Table IX with those in Table III. When $Sr_3LaCuRuO_8$ is doped with excess Sr, the unit cell parameter a shows little change, whereas c decreases significantly. In interpreting this observation we must remember that replacing La^{3+} by Sr^{2+} would be expected to increase both a and c on size grounds alone. Our neutron diffraction results show that the introduction of excess Sr introduces vacancies onto the oxide sublattice rather than oxidizing Cu^{2+} to Cu^{3+}; the refined vacancy concentration corresponds very closely to that expected if Cu^{2+} and Ru^{5+} are the only transition metal species present. The introduction of vacancies will reduce the average coordination number about the Sr/La site and hence reduce the average Sr/La–O bond length (Table IX). In order to understand the anisotropic change in the size of the Cu/Ru site, we must consider the electronic structures of the cations involved. The vacancies are confined to the O2 site in the equatorial plane of the Cu/Ru–O_6 octahedra, in a way which is reminiscent of Sr_2CuO_3 (*13*) rather than the Ruddlesden–Popper phases described above. It is unlikely that the introduction of anion vacancies will have a significant effect on the low-lying cation t_{2g} manifolds in these compounds; the high-energy e_g^* orbitals, which are directed towards the anion or vacancy, are likely to be affected more. Given that the e_g levels are empty in Ru(V), we treat the electronic structure of Ru(V): t_{2g}^3 as invariant in the discussion that follows and discuss the observed behavior in terms of

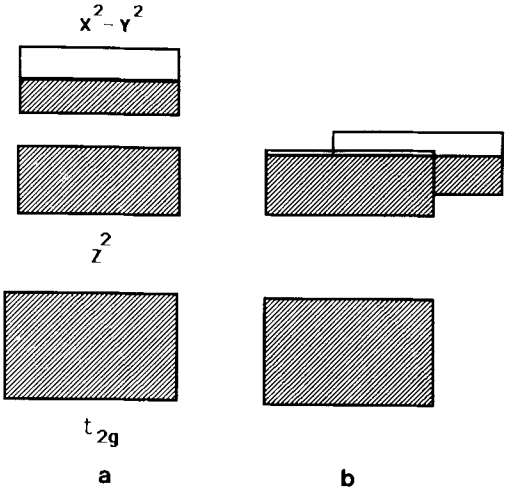

FIG. 13. Energy levels for the Cu^{2+} 3*d* bands in (a) $Sr_3LaCuRuO_8$ and (b) $Sr_{3.5}La_{0.5}CuRuO_{8-\delta}$.

the electronic structure of Cu^{2+} ($t_{2g}^6 e_g^3$). The observed bond lengths under discussion are of course the average of the Cu–O and Ru–O distances in this disordered material; we assume that the Ru–O environment is constant and that changes in the average are due to changes in the Cu–O environment. We believe that it is likely that the anion vacancies occur between pairs of Cu atoms in the disordered cation array to create a local square pyramidal environment similar to that found in Sr_2CuO_3; the local coordination of Ru(V) has been shown to be regular in a wide range of oxides (*1, 14*). When Cu^{2+} occupies a site with tetragonal symmetry ($c/a > 1$) the e_g^* band will be split into two sub-bands, the z^2 band and the x^2-y^2 band, the latter having the higher energy. Figure 13a represents the situation when the splitting is large compared to the bandwidth, Fig. 13b the reverse situation. The former is a reasonable representation of the situation in $Sr_3LaCuRuO_8$, the z^2 band being full and the x^2-y^2 band half full. When anion vacancies are present in the *ab* plane the latter band will be stabilized with respect to the z^2 band, thus approaching the situation drawn in Fig. 13b. This will result in a redistribution of electron density from the z^2 band to the x^2-y^2 band and so, given that both bands are antibonding, there is a decrease in the metal–oxygen bond lengths along *c*. The small change observed in the bond lengths perpendicular to *c* is the net effect resulting from the stabilization of the x^2-y^2 band and the consequent increase in its population. Similar arguments can be used in discussing the structural differences between $Sr_3LaCuRuO_8$ and $Sr_3LaZnRuO_8$. The x^2-y^2 band is full in the latter compound, and the Zn/Ru–O2 bonds in the *ab* plane are consequently longer than those found in the Cu compound. This increase in bond length is reflected in the unit cell parameter *a*. However, the decrease in the unit cell parameter *c* does not reflect the change in the Zn/Ru–O1 distance parallel to the *c* axis. The increase in the latter distance is a consequence of the marked decrease in the axial Sr/La–O1 distance, which is in turn necessary to conserve the total bond strength around the Sr/La site following the increase in length of the four Sr/La–O1 bonds which lie approximately perpendicular to the *c* axis. This latter increase is of course necessitated by the increase in the Zn/Ru–O2 distances. Once again our interpretation implies that the interatomic distances along the *c* axis are dictated by the bonding requirements of the atoms within the layers. The absence of cation ordering in the K_2NiF_4 phases described above is consistent with the findings of Ackerman (*15*), who prepared a large number of mixed oxides in which 50% of the 6-coordinate sites were occupied by Nb(V) or Ta(V), the remainder being occupied by another transition metal or lanthanide. No cation ordering was observed. The relatively large temperature factors listed in Table VIII are again attributable to local atomic displacements brought about by the presence of disorder.

A number of points are clearly illustrated by the electrical conductivity data plotted in

Fig. 11. First, the resistivity increases by a factor of $> 10^3$ when only half the BO_6 octahedra are occupied by a transition metal with a partially filled d shell, irrespective of whether that transition metal is Cu or Ru, thus implying that there is a significant interaction between the $3d^9$ and $4d^3$ systems. However, the interaction is not strong enough to produce a delocalized electron system, and all the materials described in this paper are semiconductors. The 3-D perovskite compounds have the highest conductivities of all the materials studied, but there is no clear difference between comparable Ruddlesden–Popper (curve iii) and K_2NiF_4 phases (curves iv and v), in which the transition metal oxidation states are essentially Cu^{2+} and Ru^{5+}. In view of the limitations of our conductivity data, it is probably unwise to attempt to explain the relatively small variations which occur between curves (iii) to (vi).

Finally, we note that our low-temperature neutron diffraction measurements did not provide evidence for the existence of long-range magnetic order in any of the compounds studied. This is particularly noteworthy in the case of the 3-D, magnetically concentrated perovskite $SrLaCuRuO_6$, and we shall investigate this point further.

Acknowledgments

We are grateful to Dr. J. K. Cockcroft for his help at ILL and to the SERC for financial support. Dr. M. Kurmoo assisted with the electrical conductivity measurements.

References

1. P. D. Battle, J. B. Goodenough, and R. Price, *J. Solid State Chem.* **46,** 234 (1983).
2. S. N. Ruddlesden and P. Popper, *Acta Crystallogr.* **11,** 54 (1958).
3. B. Toby, D. E. Cox, and P. Zolliker, unpublished work.
4. H. M. Rietveld, *J. Appl. Crystallogr.* **2,** 65 (1969).
5. P. D. Battle and C. W. Jones, *Mater. Res. Bull.* **22,** 1623 (1987).
6. P. A. Cox and P. Jason, unpublished results.
7. G. Blasse, *J. Inorg. Nucl. Chem.* **27,** 993 (1965).
8. N. F. Mott, *Philos. Mag.* **19,** 835 (1969).
9. M. A. Kastner, R. J. Birgeneau, C. Y. Chen, Y. M. Chiang, D. R. Gabbe, H. P. Jenssen, T. Junk, C. J. Peters, P. J. Picone, Tineke Thio, T. R. Thurston, and H. L. Tuller, *Phys. Rev. B.* **37,** 111 (1988).
10. P. D. Battle, T. C. Gibb, and P. Lightfoot, *J. Solid State Chem.* **84,** 237 (1990).
11. T. Nakamura and J. Choy, *J. Solid State Chem.* **20,** 233 (1977).
12. P. D. Battle, T. C. Gibb, C. W. Jones, and F. Studer, *J. Solid State Chem.* **78,** 281 (1989).
13. V. L. Teske and H. Muller-Buschbaum, *Z. Anorg. Allg. Chem.* **371,** 325 (1969).
14. P. D. Battle, C. W. Jones, and F. Studer, *J. Solid State Chem.* **90,** 302 (1991).
15. J. F. Ackerman, *Mater. Res. Bull.* **14,** 487 (1979).